Research Square

Preprints are preliminary reports that have not undergone peer review.
They should not be considered conclusive, used to inform clinical practice,
or referenced by the media as validated information.

Aerobic Exercise Enhances CXCL9-Mediated Recruitment of Universal CEA-CAR-T Cells and Antitumor Efficacy in Murine Colorectal Cancer

Jing Zhang
The Quzhou Affiliated Hospital of Wenzhou Medical University, Quzhou People's Hospital
Xin Zhou
Shandong Sport University
Ganghui Ye
Taizhou Central Hospital (Taizhou University Hospital)
Qinglu Wang
Shandong Sport University
Shixiu Wu
wushixiu@medmail.com.cn

The Quzhou Affiliated Hospital of Wenzhou Medical University, Quzhou People's Hospital

Research Article

Keywords: induced pluripotent stem cells (iPSCs), CRISPR/Cas9-mediated gene editing, universal chimeric antigen receptor T cells (U CAR-T cells), colorectal cancer (CRC), carcinoembryonic antigen (CEA)

Posted Date: November 20th, 2026

DOI: https://doi.org/10.21203/rs.3.rs-11347367/v1

License: This work is licensed under a Creative Commons Attribution 4.0 International License.
Read Full License

Additional Declarations: No competing interests reported.

Abstract

This study aimed to investigate the antitumor effects and underlying mechanisms of aerobic exercise combined with universal chimeric antigen receptor T (U CAR-T) cell therapy in colorectal cancer (CRC). First, CRISPR/Cas9-mediated knockout of NLRC5 and CIITA in induced pluripotent stem cells (iPSCs) was performed to generate universal iPSCs with reduced immunogenicity and enhanced resistance to immune rejection, which were subsequently induced to differentiate into T cells. A second-generation chimeric antigen receptor (CAR) targeting carcinoembryonic antigen (CEA) was then constructed and introduced into the differentiated T cells via lentiviral transduction to generate U CAR-T cells. In vitro experiments demonstrated that U CAR-T cells exhibited stable surface expression of CEA-CAR and potent, specific cytotoxicity against CEA-positive CRC cells. A CRC xenograft model was subsequently established in nude mice to evaluate the therapeutic efficacy of aerobic exercise combined with U CAR-T cells in vivo. No significant differences in body weight were observed among the groups, indicating that the treatment was well tolerated. Tumor inhibition increased in the following order: Ctrl < Ex<U CAR-T < Ex+U CAR-T, with the combined treatment showing the greatest antitumor efficacy. Immunohistochemical analysis revealed markedly increased infiltration of $CD3^+$, $CD4^+$, and $CD8^+$T cells in tumor tissues from the combined-treatment group. Moreover, ELISA demonstrated significantly increased levels of IL-2, TNF-α, IFN-γ, and CXCL9, whereas hematoxylin and eosin staining revealed no obvious pathological damage to major organs, including the liver and lungs. These findings suggest that aerobic exercise enhances the infiltration and activation of U CAR-T cells within the tumor microenvironment, potentially through upregulation of CXCL9, thereby alleviating immunosuppression and enhancing the antitumor efficacy of U CAR-T cell therapy. Collectively, aerobic exercise combined with U CAR-T cell therapy exhibited favorable antitumor activity and tolerability, providing experimental evidence and a potential therapeutic strategy for improving immunotherapy efficacy in CRC.

Introduction

Colorectal cancer (CRC) is the third most commonly diagnosed malignancy and the second leading cause of cancer-related mortality worldwide(1, 2).In 2020, approximately 1.88 million new cases of CRC and 915,000 CRC-related deaths were reported globally(3).In 2022, the global burden increased to approximately 1.9261 million new cases and 903,900 deaths, with 517,100 new cases and 240,000 deaths reported in China(4, 5).It is estimated that by 2050, CRC will account for approximately 2.18 million deaths worldwide, while the disability-adjusted life years (DALYs) attributable to CRC are projected to reach 41.7 million(6).In China, approximately 610,000 new CRC cases and 300,000 CRC-related deaths were reported in 2023, with a notable trend toward an increasing incidence among younger populations(7).

The 5-year survival rate of patients with advanced or metastatic CRC remains approximately 12%(8, 9), previous studies have shown that patients with colorectal cancer liver metastases (CRLM) experience a postoperative recurrence rate of 40%–50% within the first year, with a 5-year recurrence rate exceeding 60%. This high recurrence rate not only severely compromises patient prognosis but also increases the

complexity of subsequent treatments and the overall medical burden(10).Although therapeutic strategies including chemotherapy, radiotherapy, and targeted therapy have improved clinical outcomes, they remain limited by high recurrence rates, acquired drug resistance, and substantial treatment-related toxicities(11, 12).Chimeric antigen receptor T-cell (CAR-T) therapy has achieved complete response rates of 75%–90% in hematological malignancies(13).However, its therapeutic efficacy in solid tumors such as CRC remains unsatisfactory due to multiple barriers, including the immunosuppressive tumor microenvironment (TME), insufficient T-cell infiltration, and allogeneic immune rejection(14).

Carcinoembryonic antigen (CEA), a well-established tumor-associated antigen, is highly expressed in CRC tissues and elevated in the serum of patients with gastrointestinal malignancies or metastatic tumors(15, 16),while exhibiting limited expression in normal tissues, making it an ideal target for immunotherapy. Previous studies have demonstrated that CEA-targeted CAR-T cell therapy can induce sustained antitumor immune responses in colorectal cancer (17).Universal chimeric antigen receptor T (U CAR-T) cells generated through the combination of CRISPR/Cas9-mediated gene editing and induced pluripotent stem cells (iPSCs) can reduce immune rejection by disrupting key genes such as T-cell receptor (TCR)-related genes, thereby enhancing the potential for “off-the-shelf” cell therapy applications (18, 19).Regular moderate-intensity aerobic exercise has been reported to reduce the risk of CRC development by approximately 10%(20),and improve the TME by promoting vascular normalization, upregulating CXCL9 expression, and enhancing $CD8^+$ T-cell recruitment(21).

Based on these considerations, we sought to generate CEA-targeted U CAR-T cells and investigate whether aerobic exercise could promote U CAR-T cell infiltration into tumors and enhance their antitumor activity through the CXCL9 axis, thereby providing experimental evidence and a potential therapeutic strategy for combination immunotherapy in CRC.

Materials and Methods

Generation of iPSC-T Cells Using CRISPR/Cas9 Technology

Human induced pluripotent stem cells (hiPSCs) derived from healthy donors were used as the starting material in this study (22),The generation of hiPSCs was strictly performed according to the procedures described in Chinese patent (ZL202210624792.4). After approval by the Shandong Sport University ethics committee under the project titled ‘Immune Checkpoint Blockade and the Development and Clinical Evaluation of a Universal CEA-Targeted CAR-T Cell Product for Colorectal Cancer’ (Approval No. 2021041; date of approval: 01-12-2021), all hiPSCs were cultured in ncTarget medium supplemented with Nuwacell™ Blebbistatin inhibitor throughout the experimental process. Cas9-mediated geneediting was employed to generate universal iPSCs and their derived T cells(23).

Based on a previously authorized patent (ZL202210624795.8), CRISPR/Cas9 knockout vectors were designed and constructed. Specific guide RNAs (gRNAs) targeting the NLRC5 and CIITA genes were

designed (NLRC5: AGCATCCTTAGACACTCCGGAGG; CIITA: TAGAAGTGGTAGAGGCACAGGGG), and a dual-target knockout vector, p2U6gRNA-Cas9-GFP-NLRC5-CIITA, was generated. The vector (1μg) was introduced into 2×10^5 hiPSCs using the Lonza 4D-Nucleofector system. Following monoclonal selection, PCR amplification, and Sanger sequencing, universal hiPSC clones carrying frameshift mutations in both NLRC5 and CIITA were obtained.

The pluripotency of the edited hiPSCs was evaluated by immunofluorescence staining for pluripotency markers, including Nanog, Oct4, and SOX2. Flow cytometry, whole-genome sequencing, and exome sequencing were further performed to assess gene-editing efficiency, potential off-target effects, and maintenance of stem cell characteristics.

Universal iPSC-derived T (iPSC-T) cells were subsequently generated through a stepwise differentiation protocol. Briefly, on day 2 of differentiation, cells were cultured with induction factors including 50ng/mL basic fibroblast growth factor (bFGF), 50ng/mL vascular endothelial growth factor (VEGF), and 40ng/mL bone morphogenetic protein 4 (BMP4). On day 5, 50ng/mL stem cell factor (SCF) was added, followed by supplementation with 10ng/mL FMS-like tyrosine kinase 3 ligand (FLT-3L) and 30ng/mL thrombopoietin (TPO) on day 7. After 14 days of induction, hematopoietic progenitor cells were generated. These cells were subsequently co-cultured with OP9-DL1 cells and differentiated into T cells in the presence of 10ng/mL interleukin-7 (IL-7) and 30ng/mL FLT-3L. Following CD3 antibody-mediated activation, universal iPSC-T cells were obtained.

The alloreactivity of generated iPSC-T cells was evaluated using a 1μM carboxyfluorescein succinimidyl ester (CFSE) labeling assay to assess their stimulatory capacity toward allogeneic $CD4^+$ and $CD8^+$T cells. HLA-reactive $CD8^+$T cells were expanded using phytohemagglutinin (PHA, 2μg/mL), IL-7 (10ng/mL), and IL-15 (5ng/mL). Finally, a ^{51}Cr release assay was performed to evaluate the specific cytotoxic activity of iPSC-T and CEA-CAR-iPSC-T cells against CRC cells. The ability of NLRC5-deficient iPSC-T cells to evade immune attack mediated by HLA-reactive T cells was also assessed, thereby systematically validating the immunogenicity, functional activity, and safety profile of universal iPSC-T cells.

Generation of Universal CEA-CAR-T Cells

In this study, universal CEA-CAR-T cells were generated using 293T, HT29, SW480, Jurkat, and CTLL-2 cell lines, which were cultured under standard conditions at 37°C with 5% CO_2. A second-generation CEA-CAR construct was designed, consisting of a CEA-specific single-chain variable fragment (scFv), an IgG4 hinge region, a CD8α transmembrane domain, a 4-1BB costimulatory domain, and a CD3ζ signaling domain(24),the CAR sequence was cloned into a piggyBac (PB) transposon vector. HEK293T cells were used as packaging cells for lentiviral production. When the cell confluency reached 60%–85%, lentiviral packaging was performed using the SweTransDNA transfection system. Briefly, each well was transfected with 2μg of CAR plasmid, 0.8μg of PCDH plasmid, 0.6μg of RSV plasmid, 0.4μg of RPE plasmid, and 0.2μg of MD2G plasmid. Viral supernatants were collected 24–48h after transfection. Following filtration through a 0.45μm membrane, the viral supernatants were mixed with 5×

concentration solution at a ratio of 4:1 and incubated at 4°C for more than 2h. The viral particles were subsequently concentrated by centrifugation at 8000 g for 10–15min and stored at -80°C until further use.

Peripheral blood mononuclear cells (PBMCs) were isolated by Ficoll density gradient centrifugation, and $CD3^+$T cells were purified using CD3 MicroBeads magnetic separation. The isolated T cells were expanded in X-VIVO15 medium supplemented with 100μg/mL IL-2 and 5% serum. Prior to transduction, universal iPSC-T cells were adjusted to a density of 0.7×10^6 cells/mL and seeded into 24-well plates pre-coated with TA activator for 24 h. The viral infection dose was calculated according to the formula: viral volume=cell number×MOI÷viral titer (TU). Subsequently, the cell density was adjusted to 0.7×10^7 cells/mL for lentiviral transduction.

After 24h of infection, the culture medium was replaced with fresh medium, and cells were continuously cultured with 100–600 IU/mL IL-2 for an additional 48-72h. CAR expression and cellular morphology were dynamically monitored using fluorescence microscopy. Cell density was maintained within the range of 0.7×10^6-2×10^6 cells/mL during expansion. After stable cell growth was achieved, cells were further passaged and expanded to obtain universal iPSC-T cells with high CEA-CAR expression, which were subsequently used for in vitro and in vivo antitumor functional studies.

Characterization of Generated Universal CEA-CAR-T Cells

To evaluate the proliferative capacity and in vitro cytotoxic activity of the generated U CAR-T cells, FarRed-APC fluorescent dye was first used to label CEA-CAR-T cells at a dilution ratio of 1:1000. Subsequently, 1×10^6 labeled cells were co-cultured with LOVO cells at an effector-to-target (E) ratio of 1:1 for 3days. Changes in FarRed fluorescence intensity were detected using a FACS Fortessa flow cytometer to evaluate the proliferative capacity of U CAR-T cells.

The in vitro cytotoxicity of U CAR-T cells was further assessed using the CellTiter-Lumi™ luminescence-based assay. Briefly, 2×10^4 CEA-positive target cells were seeded into 96-well plates and co-cultured with control T cells or U CAR-T cells at different E ratios (1:1, 3:1, and 9:1) for 24h. The results demonstrated that target cells were almost completely eliminated at E ratios of 3:1 and 9:1. At an E ratio of 1:1, the average killing rate of control T cells was 12.58%, whereas U CAR-T cells exhibited an average cytotoxicity of 35.75%, representing an approximately 2.8-fold increase compared with control T cells.

The cytotoxicity rates of U CAR-T cells in individual replicate wells were 37.36%, 45.58%, and 34.14%, respectively, which were significantly higher than those observed in control T cells (14.15%, 13.25%, and 10.34%, respectively). These results indicate that the generated U CAR-T cells possess robust proliferative activity and enhanced in vitro CEA-specific antitumor cytotoxicity.

Detection of CEA Expression in Colorectal Cancer Cells

To determine the expression level of CEA in colorectal cancer cells, SW480 and HT-29 cells were recovered from liquid nitrogen and cultured in complete Dulbecco's modified Eagle's medium (DMEM) supplemented with 10% fetal bovine serum (FBS) and 1% penicillin–streptomycin. After the cells reached a stable growth state, they were harvested by trypsin digestion, centrifuged, and resuspended in 100μL phosphate-buffered saline (PBS). The cells were then incubated with a CD66e (CEA) flow cytometry antibody at 4°C in the dark.

In Vivo Therapeutic Evaluation in a CRC Mouse Model

All animal experiments were approved by the Animal Ethics Committee of Shandong Sport University under the project titled 'Immune Checkpoint Blockade and the Development and Clinical Evaluation of a Universal CEA-Targeted CAR-T Cell Product for Colorectal Cancer' (Approval No. 2021041; date of approval: 01-12-2021) and were conducted in accordance with the National Institutes of Health (NIH) Guide for the Care and Use of Laboratory Animals. This study was designed and is reported in compliance with the Animal Research: Reporting of In Vivo Experiments (ARRIVE) 2.0 guidelines (https://arriveguidelines.org). Based on an a priori power analysis performed using G*Power software, forty 6-week-old female NYG immunodeficient mice weighing 20-25g were selected and acclimatized for 1 week before establishment of the CRC tumor model. All mice were housed under specific pathogen-free (SPF) conditions in individually ventilated cages (IVCs) at a controlled temperature of 22–24°C and relative humidity of 40–60%, with a 12-h light/dark cycle; autoclaved bedding, irradiated food, and sterile water were provided ad libitum, and cages were changed within a sterile biosafety cabinet.

According to the experimental objectives, the mice were divided into two independent cohorts, with 20 mice in each cohort. Both cohorts were subjected to identical grouping strategies and treatment protocols. In each cohort, mice were randomly assigned into four groups (n = 5): the control group (Ctrl), aerobic exercise group (Ex), U CAR-T treatment group (U CAR-T), and aerobic exercise combined with U CAR-T treatment group (Ex + U CAR-T). Mice in the Ctrl and Ex groups received intraperitoneal injection of an equal volume of PBS, whereas mice in the U CAR-T and Ex + U CAR-T groups received intraperitoneal administration of 1×10^7 U CAR-T cells on days 2, 9, and 16 after tumor establishment (25).Mice in the first cohort received continuous intervention for 21 days. The second cohort, consisting of another 20 mice, was used for survival analysis.

U CAR-T Cell Therapy Combined with Aerobic Exercise Intervention

Before cell administration, U CAR-T cells were counted using a hemocytometer. The cell concentration was calculated based on the dilution factor and counting results to ensure accurate administration of the required cell dose. Intraperitoneal injection was performed under sterile conditions. Briefly, mice were anesthetized with 2% lidocaine (100 mg/kg administered by intraperitoneal injection); the depth of anesthesia was confirmed by the absence of the pedal withdrawal reflex before the procedure. The cell

suspension was slowly injected into the abdominal cavity using a 27-gauge needle. After injection, mice were placed in a recovery chamber at 37°C and monitored until full recovery, and their general condition was observed for 24h.

The aerobic exercise intervention protocol was designed according to previously reported methods(26).Aerobic training was performed using an electric treadmill equipped with a 0.3mA safe electrical stimulation device. The exercise parameters were set as follows: running speed of 9m/min, 30 min per session, 5 sessions per week, for a continuous period of 3 weeks.

During the intervention period, the general condition and exercise tolerance of mice were monitored daily, and body weight was recorded every 48h. Predefined humane endpoints included inability to access food or water, persistent recumbency, marked lethargy, body weight loss exceeding 20%, or excessive tumor burden; mice reaching any humane endpoint were euthanized immediately as described below. At the end of the experiment, the remaining mice were euthanized, and tumor tissues were isolated. Changes in tumor volume and survival status were subsequently evaluated to determine the therapeutic effects of aerobic exercise and U CAR-T cell therapy, either alone or in combination, against CRC.

Tumor Monitoring and Sample Collection

Tumor volume was measured every 3 days using a vernier caliper by recording the longest diameter (L) and shortest diameter (W), and tumor volume was calculated according to the formula: $V = 0.5 \times L \times W^2$. Tumor growth was continuously monitored throughout the experimental period.

After completion of all interventions, 20 mice were euthanized by intraperitoneal injection of sodium pentobarbital at a dose of 200 mg/kg body weight. Mice in the survival cohort that reached the predefined humane endpoints were euthanized using the same method. Death was confirmed by cessation of respiration and heartbeat. Subsequently, the mice underwent left ventricular perfusion with 15mL of pre-cooled heparinized PBS to remove residual blood. Whole blood samples were collected from the orbital venous plexus and centrifuged at 3000g for 15 min to obtain serum samples, which were stored at -80°C until further analysis. Tumor tissues were collected for Hematoxylin and Eosin (HE) staining.

Following dissection, a portion of tumor tissues and spleens were rapidly frozen in liquid nitrogen, while another portion was fixed in 4% paraformaldehyde for subsequent immunofluorescence and immunohistochemical analyses. All samples were labeled with standardized identification codes and stored under specified conditions to ensure the reliability and reproducibility of experimental results.

Enzyme-Linked Immunosorbent Assay

Prior to the assay, the CXCL9 ELISA kit was equilibrated at room temperature (20–25°C) for 10min. The standard stock solution (2000pg/mL) was prepared by dissolving the lyophilized standard with 1mL of

universal diluent, followed by incubation for 15min and thorough mixing. A series of standard solutions was prepared using a two-fold serial dilution method. Briefly, 500μL of the previous concentration was sequentially transferred into seven EP tubes preloaded with 500μL of universal diluent, generating eight concentration gradients ranging from 2000 to 31.25pg/mL, along with a blank control (0pg/mL).

The horseradish peroxidase (HRP)-conjugated detection antibody working solution was prepared immediately before use. The 100×concentrated solution was centrifuged at 1000×g for 1 min and diluted 1:100 with universal diluent. The 1×washing buffer was prepared by diluting the 20× concentrated solution at a ratio of 1:19 (10mL concentrate + 190 mL distilled water). If crystallization occurred, the solution was completely dissolved at room temperature before use.

For the ELISA procedure, the required microplate strips were removed, while the remaining strips were sealed and stored at 4°C. Subsequently, 100μL of samples (recommended to be diluted at least 1-fold to reduce matrix effects), standards, or blank diluent were added to each well in duplicate. The plate was incubated at 37°C for 60min. After incubation, the plate was washed three times with 300μL of 1×washing buffer per well, with a 1min standing time after each wash, followed by plate inversion and gentle drying.

Then, 100μL of HRP-conjugated detection antibody working solution was added to each well, followed by incubation at 37°C for 60min. The plate was subsequently washed five times, and 90μL of tetramethylbenzidine (TMB) substrate solution was added for color development at 37°C in the dark for 15min. The reaction was terminated by adding 50μL of stop solution, and the optical density (OD) values were immediately measured at 450nm.

In addition, mouse serum samples were analyzed using ELISA kits provided by Wuhan Fine Biotech Co., Ltd. according to the manufacturer's instructions. The concentrations of inflammatory cytokines, including IFN-γ, IL-2, and TNF-α, were quantitatively determined.

Hematoxylin and Eosin Staining

Histological sections of tumor tissues were prepared strictly according to the established standard operating procedure (SOP). For paraffin-embedded sections, deparaffinization and rehydration were performed using an environmentally friendly dewaxing solution (I and II, 20min each), followed by graded ethanol treatment (100% ethanol I and II, 5min each;75% ethanol,5min) and rinsing with running water. For frozen sections, the sections were equilibrated to room temperature from − 20°C and fixed in fixation solution for 15min, followed by rinsing with running water. Both paraffin-embedded and frozen sections were subsequently treated with a high-definition HE staining pretreatment solution for 1 min. Hematoxylin staining was performed for 3-5min, followed by water washing, differentiation, and bluing. The sections were then dehydrated with 95% ethanol for 1 min and counterstained with eosin for 15s. Subsequently, the sections were dehydrated and cleared using anhydrous ethanol, n-butanol, and xylene in two sequential steps (2 min per step), mounted with neutral balsam, and examined and imaged under a light microscope.

For the cell-based assay, SW480 and HT-29 cells were recovered and expanded in DMEM supplemented with 10% FBS and 1% penicillin-streptomycin. Cells were harvested by trypsin digestion and resuspended in PBS, followed by incubation with a CD66e antibody at 4°C. After washing to remove unbound antibody, the surface expression of CEA on SW480 and HT-29 cells was analyzed using a FACS Fortessa flow cytometer.

Immunohistochemistry

The immunohistochemical procedures described in this study involved standardized sample pretreatment and subsequent staining protocols for various types of specimens. For paraffin-embedded sections or tissue microarrays, graded treatment with an environmentally friendly dewaxing solution was first performed to ensure complete deparaffinization, followed by rehydration through a graded series of anhydrous ethanol to distilled water. Frozen sections were baked at 37°C for 10-20min for dehydration and fixed in methanol for 30min, followed by three washes with pH 7.4 PBS. For cell coverslips, after fixation and washing, all samples except those subjected to membrane protein staining were treated with permeabilization solution at room temperature for 20min, followed by three washes with PBS.

For suspended cells, cells were first collected by centrifugation at 2800rpm for 5min at 4°C, with centrifugation at 3000rpm for 10min when necessary. After removal of the supernatant, the cells were fixed with 4% paraformaldehyde. The fixative was subsequently removed by centrifugation, and the cell pellet was resuspended in PBS according to its volume and used to prepare cytological smears. When the cell pellet was small, the suspension was concentrated and drops were applied within a small circle pre-marked with a hydrophobic barrier pen. When the cell pellet was relatively large, the volume of PBS was appropriately increased to dilute the suspension and ensure a uniform smear thickness; serial dilution was performed when necessary. After uniform cell distribution was confirmed microscopically, the smears were allowed to air-dry naturally. Fixative was then added within the marked circle, and the smears were fixed at room temperature for 20min. After washing, permeabilization solution was added and the samples were incubated for 20min, whereas permeabilization was omitted for membrane protein staining. The samples were subsequently washed with PBS.

For the staining procedure, tissue sections underwent antigen retrieval, with particular care taken to prevent the sections from drying, followed by cooling and three washes with PBS. Antigen retrieval was omitted for cell coverslips and cytological smears. Endogenous peroxidase activity was blocked by incubation with 3% methanol-hydrogen peroxide solution at room temperature in the dark for 25 min, followed by three washes with PBS. The samples were then blocked with 3% bovine serum albumin (BSA) at room temperature for 30min; rabbit serum was used instead of BSA when the primary antibody was derived from goat. Subsequently, the diluted primary antibody was added, and the samples were incubated overnight at 4°C in a humidified chamber.

On the following day, the samples were washed three times with PBS and incubated with an horseradish peroxidase (HRP)-conjugated secondary antibody at room temperature for 50 min. After further washing, freshly prepared 3,3'-diaminobenzidine (DAB) substrate was added for chromogenic development. Color

development was monitored microscopically and immediately terminated with running water when brown-yellow positive staining became visible. The sections were then counterstained with hematoxylin for 3min, followed by differentiation, bluing, and rinsing with running water.

Finally, tissue sections and cytological smears were dehydrated through a graded ethanol series from 75% to anhydrous ethanol, followed by transition through n-butanol and clearing with xylene before mounting. Cell coverslips were dehydrated through a graded ethanol series, air-dried, and mounted in an inverted orientation using neutral balsam. All samples were examined and evaluated under a bright-field light microscope.

Statistical Analysis

All statistical analyses were performed using SPSS version 26.0 (IBM Corp, Armonk, NY, USA). Before statistical analysis, the data were assessed for normality and homogeneity of variances. Data are presented as the mean±standard deviation (mean ± SD). Bar graphs were generated using GraphPad Prism version 7.0 (GraphPad Software, San Diego, CA, USA). Differences among multiple groups were analyzed using one-way analysis of variance (ANOVA), whereas comparisons between two groups were performed using the independent-samples t-test. Statistical significance was determined based on the corresponding P values, with $P < 0.05$ considered statistically significant and $P < 0.01$ considered highly significant.

Results

Successful Generation of Universal iPSCs

To confirm the successful generation and culture status of the NLRC5-CIITA double-knockout (dKO) iPSC cell lines, the cells were first expanded, serially passaged, and characterized. PCR sequencing analysis showed that both the $NLRC5^{KO}$ and $CIITA^{KO}$ iPSC cell lines carried homozygous mutations (Fig. 1A). Meanwhile, during culture, the cells exhibited colony-like growth with well-defined margins and maintained a healthy growth state, and mycoplasma testing was negative(Fig. 1B). Further agarose gel electrophoresis showed that the $NLRC5^{KO}$ fragment was approximately 850 bp in length, whereas the $CIITA^{KO}$ fragment was approximately 647 bp in length (Fig. 1C).Immunofluorescence staining revealed strong expression of the pluripotency markers Nanog, OCT4, and SOX2 in dKO iPSCs (Fig. 1D). Collectively, these results demonstrate that the $NLRC5^{KO}$/$CIITA^{KO}$ genetically modified universal iPSCs retained pluripotent characteristics.

Generation and Characterization of Universal iPSC-T Cells

To reduce HLA-I-mediated immunogenicity and prevent graft-versus-host disease (GVHD), the NLRC5 gene was knocked out in iPSC-T cells using CRISPR/Cas9 technology(27–29). A schematic illustration of the generation of $NLRC5^{KO}$ iPSC-T cells and the co-culture experiment with allogeneic $CD8^{+}$T cells is

shown (Fig. 2A). CFSE-labeled allogeneic $CD8^+$T cells were co-cultured with WT or $NLRC5^{KO}$ iPSC-T cells for 7–8 days (n = 4). The WT group induced marked proliferation of allogeneic $CD8^+$T cells, whereas no significant CFSE dilution was observed in the $NLRC5^{KO}$ group, indicating that $NLRC5^{KO}$ iPSC-T cells failed to effectively activate allogeneic $CD8^+$T cells (Fig. 2B). The results of the ^{51}Cr release cytotoxicity assay showed that, at effector-to-target (E) ratios of 2.5:1, 5:1, 10:1, and 20:1, WT iPSC-T cells were subjected to substantial immune-mediated cytotoxicity by allogeneic $CD8^+$T cells, whereas $NLRC5^{KO}$ iPSC-T cells effectively escaped immune-mediated killing (Fig. 2C). These results demonstrate that NLRC5 knockout significantly reduces the HLA-I-dependent immunogenicity of iPSC-T cells, providing a foundation for the development of low-immunogenicity universal CAR-T cells.

To further reduce the immunogenicity of iPSC-T cells, the CIITA gene, a key transcriptional regulator of HLA-II expression, was additionally knocked out based on the NLRC5-deficient background, resulting in the generation of NLRC5/CIITA double-knockout (dKO) iPSC-T cells (28, 30, 31).The schematic workflow for the generation of dKO iPSC-T cells and the evaluation of their immunogenicity toward allogeneic $CD4^+$T cells is shown (Fig. 3A).

CFSE-labeled allogeneic $CD4^+$T cells were co-cultured with $NLRC5^{KO}$ or dKO iPSC-T cells for 7 days (n = 7). The $NLRC5^{KO}$ group induced proliferation of allogeneic $CD4^+$T cells and increased CD40L expression, whereas the dKO group showed no obvious CFSE dilution or upregulation of CD40L expression, indicating that dKO iPSC-T cells were unable to effectively activate allogeneic $CD4^+$T cells (Fig. 3B).

The results of the ^{51}Cr release cytotoxicity assay are shown (Fig. 3C). Under different effector-to-target (E) ratios of 2.5:1, 5:1, 10:1, and 20:1, WT iPSC-T cells were significantly recognized and attacked by allogeneic $CD4^+$T cells, whereas dKO iPSC-T cells effectively escaped immune-mediated cytotoxicity.

Collectively, these results demonstrate that CIITA knockout significantly reduces HLA-II-dependent immunogenicity of iPSC-T cells and further enhances their immune evasion capacity, supporting the development of low-immunogenicity universal CAR-T cell products.

Generation, Characterization, and In Vitro Antitumor Activity of Universal CEA-CAR-T Cells

To establish a universal CAR-T cell system targeting CEA, the CAR vector design and viral delivery system were first optimized. Flow cytometric analysis revealed differential CEA expression levels among CRC cell lines. HT29 cells exhibited 73.1% CEA positivity, whereas SW480 cells showed a higher CEA expression level of 99.9%. Therefore, SW480 cells were selected as CEA-positive target cells for subsequent functional assays (Fig. 4A-B).

A four-plasmid lentiviral packaging system consisting of pCDH, pRRE, pRSV, and pMD2.G at a ratio of 4:3:2:1 was used to co-transfect 293T cells. After 48 h, the fluorescence-positive rate exceeded 90%, indicating successful lentiviral packaging (Fig. 4C). The construction of U CAR-T cells was further

validated. GFP-labeled lentiviral transduction resulted in stable T-cell survival, and flow cytometric analysis demonstrated that the CEA-CAR expression rate increased from 0.95% to 51.23%, confirming the successful generation of highly efficient CEA-targeted CAR-T cells (Fig. 4D-E).

Collectively, these results demonstrate the establishment of a stable and feasible CEA-targeted universal CAR-T cell generation system. Subsequently, SW480 cells were co-cultured with control T cells or U CAR-T cells at an effector-to-target ratio of 1:1 for 24 h to evaluate cytotoxic activity. U CAR-T cells exhibited an average killing efficiency of 35.75% against CEA-positive target cells, which was significantly higher than that observed in the control T-cell group (12.58%) (Fig. 4F). These findings confirm the specific cytotoxic activity of U CAR-T cells against CEA-positive CRC cells and demonstrate their potent antitumor capability in vitro.

U CAR-T Cell Therapy Combined with Aerobic Exercise Exhibits Enhanced Antitumor Activity in a CRC Model

After 21 days of treatment, mice were euthanized, and tumor tissues were excised, measured, and weighed. The tumor volume measurements showed that the Ex + U CAR-T group had the smallest tumor volumes among the four groups (Fig. 5A). Quantitative analysis of tumor weight and volume demonstrated that the Ex group ($P < 0.05$), U CAR-T group ($P < 0.01$), and Ex + U CAR-T group all exhibited significant inhibition of tumor growth. Notably, tumor suppression was greater in the Ex + U CAR-T group than in either the Ex or U CAR-T group ($P < 0.05$) (Fig. 5B-C).

To evaluate the therapeutic efficacy and safety of U CAR-T cell therapy, body weight was monitored continuously for 21days. No significant differences in body weight gain were observed among the groups ($P > 0.05$), suggesting that the treatments did not cause obvious systemic toxicity (Fig. 5D). After 21days, blood samples were collected from CRC-bearing mice and centrifuged at 15,000rpm for 10min to obtain serum. ELISA was performed to determine the serum levels of IL-2, TNF-α, and IFN-γ, as well as CXCL9 protein expression in tumor tissues.

Survival was monitored in CRC-bearing mice receiving different treatments (Fig. 5E). Compared with the Ctrl group, the Ex group showed significantly increased levels of IL-2 and IFN-γ ($P < 0.05$), whereas TNF-α was more markedly increased ($P < 0.01$), suggesting that aerobic exercise enhanced the systemic immune response. Compared with the Ex group, the U CAR-T group exhibited further increases in IL-2 and IFN-γ levels ($P < 0.01$), indicating enhanced T-cell activation. In the Ex + U CAR-T group, IL-2 and IFN-γ levels were significantly higher than those in the U CAR-T group ($P < 0.01$), while TNF-α levels were also significantly increased ($P < 0.05$) (Fig. 5F-H). These findings indicate that aerobic exercise may enhance the TME and promote U CAR-T cell infiltration and functional activation, thereby contributing to the enhanced antitumor activity observed with the combined treatment.

CXCL9 protein expression in tumor tissues was subsequently analyzed. The Ex group exhibited significantly higher CXCL9 expression than the Ctrl group ($P < 0.01$), suggesting that aerobic exercise enhanced CXCL9 production within the TME. No significant difference was observed between the U CAR-

T and Ctrl groups ($P > 0.05$), suggesting that CXCL9 expression may remain limited under the suppressive TME. Notably, CXCL9 expression in the Ex + U CAR-T group was further significantly increased compared with that in the Ex group ($P < 0.05$) (Fig. 5I). These findings suggest that the combined treatment may promote T-cell infiltration and enhance the activation of $CD8^+$T cells and M1 macrophages through the CXCL9/CXCR3 axis, thereby promoting IFN-γ release and establishing a positive immune amplification loop.

U CAR-T Cell Therapy Combined with Aerobic Exercise Remodels the

TME and Enhances Antitumor Activity

Histological changes in tumor and major organs were evaluated in mice from each treatment group. Tumor, liver, and lung tissues were subjected to HE staining (Fig. 6). In the Ctrl group, tumor cells were densely arranged and exhibited a disorganized tissue architecture. In the U CAR-T group, tumor cell density was reduced, accompanied by increased immune cell infiltration, indicating antitumor activity of U CAR-T cell therapy. Notably, the Ex + U CAR-T group exhibited more extensive tumor tissue destruction and the most pronounced immune cell infiltration, suggesting that aerobic exercise may improve the TME and enhance U CAR-T cell infiltration and sustained antitumor activity.

Histological examination of the liver showed that all four groups maintained the typical hepatic lobular architecture, with orderly arrangement of the central veins and hepatic cords and no apparent necrosis or inflammatory cell infiltration. In the lung tissues, the alveolar architecture remained intact with clear alveolar septa, and no obvious edema, hemorrhage, or fibrosis was observed. These findings indicate that U CAR-T cell therapy, either alone or in combination with aerobic exercise, exerted antitumor effects without causing apparent structural damage to the liver or lungs, suggesting favorable in vivo tolerability and safety.

U CAR-T Cell Therapy Enhances the Infiltration of $CD3^+$, $CD4^+$, and $CD8^+$ T Cells in Tumor Tissues

To investigate the antitumor effects of Ex + U CAR-T cell therapy in CRC-bearing mice, the distribution of U CAR-T cells within tumor tissues was evaluated, with particular emphasis on the infiltration of total T cells ($CD3^+$), helper T cells ($CD4^+$), and cytotoxic T cells ($CD8^+$). As shown (Fig. 7), the Ex + U CAR-T group exhibited increased areas and numbers of T-cell infiltration compared with the other three groups, indicating that the administered U CAR-T cells successfully reached the tumor tissues and contributed to tumor suppression.

CD3 staining revealed almost no specific positive signals in the Ctrl and Ex groups, whereas scattered $CD3^+$ cells were observed in the U CAR-T group, accounting for 10.03% of the positive staining area. In contrast, the Ex + U CAR-T group exhibited a markedly increased $CD3^+$ staining area (19.96%), suggesting that aerobic exercise may facilitate the migration and accumulation of U CAR-T cells within tumor tissues by alleviating physical barriers associated with solid tumors (Fig. 7A).

Further analysis of the $CD4^+$T-cell subset showed that the positive staining area in the combined-treatment group (24.21%) was substantially higher than that in the U CAR-T group (11.31%), suggesting that aerobic exercise may promote the recruitment of T cells through the CXCL9 axis and thereby contribute to TME remodeling. Similarly, the $CD8^+$ staining area reached 13.23% in the U CAR-T group and increased to 38.51% in the Ex + U CAR-T group, indicating enhanced infiltration of cytotoxic T cells into the TME.

Quantitative analysis of $CD3^+$, $CD4^+$, and $CD8^+$ positive cells further demonstrated that the positive cell rates in the Ex + U CAR-T group were 71.25%, 58.21%, and 91.55%, respectively, all of which were higher than those observed in the other groups. The corresponding positive rates were 25.84%, 21.63%, and 27.76% in the Ctrl group; 36.50%, 35.02%, and 48.85% in the Ex group; and 48.92%, 49.28%, and 73.71% in the U CAR-T group (Fig. 7B-D). These findings suggest that aerobic exercise promotes immune-cell infiltration within the TME and may facilitate the transition from an immunologically “cold” tumor to a “hot” tumor.

Collectively, these findings suggest that aerobic exercise does not directly exert cytotoxic effects on tumor cells but may enhance the accumulation of $CD4^+$ and $CD8^+$T cells, particularly the infiltration of $CD8^+$ effector T cells, thereby converting an immunosuppressive “cold” tumor microenvironment into a more immune-active “hot” tumor microenvironment. This combined therapeutic strategy may improve the recruitment and spatial distribution of effector T cells within tumors, thereby facilitating their penetration into tumor tissues and supporting sustained tumor-specific cytotoxic activity.

Discussion

This study addressed the key challenges limiting the application of CAR-T cell therapy in solid tumors, including the immunosuppressive TME in CRC(32, 33).We generated low-immunogenicity U CAR-T cells derived from iPSCs and further investigated the antitumor effects and potential mechanisms of combining aerobic exercise with U CAR-T cell therapy in CRC. First, a low-immunogenicity iPSC platform was established using a dual-gene knockout strategy targeting NLRC5 and CIITA. The results showed that gene editing did not compromise the pluripotency of iPSCs, with stable expression of stemness markers, including Nanog, OCT4, and SOX2. Following directed differentiation, NLRC5 knockout effectively reduced HLA-I-mediated recognition by allogeneic $CD8^+$T cells, whereas subsequent CIITA knockout further suppressed HLA-II-associated immune responses mediated by $CD4^+$T cells, thereby enhancing the immune-evasive capacity of the cells. The ^{51}Cr release assay further confirmed that the double-knockout U CAR-T cells effectively resisted attack by allogeneic T cells, providing a stable cellular source for the development of universal CAR-T cell therapy. Based on this platform, we constructed a second-generation CAR vector targeting CEA and successfully generated U CAR-T cells with stable CEA-CAR expression, with a positive rate of 51.23%. In vitro experiments demonstrated that U CAR-T cells specifically recognized CEA-high-expressing CRC cells and exhibited enhanced cytotoxic activity, indicating favorable target specificity and antitumor potential.

TME remains a major barrier to the efficacy of CAR-T cell therapy in solid tumors(34). Previous studies have shown that an anti-PD-L1–interleukin-12(IL-12) engineering strategy may enhance the clinical efficacy and safety of CAR-T cells in various solid tumors(35).In addition, the clinical efficacy of CAR-T cell therapy varies among tumor types, and clinical trials in solid tumors have generally yielded limited therapeutic benefits. For example, although B7-H3 CAR-T cell therapy has demonstrated a favorable safety profile in patients with diffuse intrinsic pontine glioma, it has not induced complete responses(36).Similarly, CD19/GCC dual-targeted CAR-T cell therapy for metastatic CRC has achieved an objective response rate of 40%, but complete responses have remained uncommon. These findings highlight the need for strategies that can improve CAR-T cell infiltration and antitumor activity within the immunosuppressive TME.

In the present study, aerobic exercise was introduced as an adjunctive intervention to U CAR-T cell therapy(37).The animal experiments demonstrated that the Ex + U CAR-T group exhibited the most pronounced tumor suppression, which was greater than that observed with either aerobic exercise or U CAR-T cell therapy alone, suggesting a potential synergistic antitumor effect between the two interventions. Notably, the combined treatment significantly increased the levels of IL-2, TNF-α, and IFN-γ and promoted CXCL9 expression in tumor tissues, suggesting that aerobic exercise may facilitate U CAR-T cell infiltration through the CXCL9/CXCR3 signaling axis and thereby enhance $CD8^+$T-cell-mediated antitumor immunity. Histological and immunohistochemical analyses further showed reduced tumor cell density and increased infiltration of $CD3^+$, $CD4^+$, and $CD8^+$T cells following combined treatment, with the $CD8^+$T-cell positivity rate reaching 91.55%. These findings suggest that aerobic exercise may contribute to remodeling the TME and enhancing the accumulation of effector T cells within tumor tissues, thereby improving the antitumor activity of U CAR-T cell therapy. Meanwhile, no obvious abnormalities were observed in body weight or the major organs of the treated mice, indicating favorable tolerability of the combined treatment strategy. Collectively, these findings provide experimental evidence supporting aerobic exercise as a potential adjunctive strategy for enhancing U CAR-T cell therapy in CRC.

Although the present study demonstrated favorable antitumor effects of combining aerobic exercise with U CAR-T cell therapy in CRC, several limitations remain to be addressed. First, the strategy for U CAR-T cell generation should be further optimized. Optimization of the CAR architecture, incorporation of additional key gene-editing targets, and improvement of the long-term persistence of U CAR-T cells in vivo may enhance their adaptability and antitumor activity within the complex TME of solid tumors. Second, the range of experimental models should be expanded. CRC cell lines with different levels of CEA expression, together with organoid models and patient-derived xenograft (PDX) models, could be incorporated to systematically evaluate the therapeutic efficacy of U CAR-T cells across different CRC subtypes. In addition, the NYG immunodeficient mouse model used in the present study cannot fully recapitulate the intact human immune microenvironment. Future studies should therefore establish immune-reconstituted or humanized mouse models to further evaluate the long-term therapeutic efficacy, safety, and immunomodulatory effects of the combined treatment. These approaches may

provide a more comprehensive assessment of the translational potential of aerobic exercise combined with U CAR-T cell therapy for CRC.

Regarding the exercise intervention, the present study employed only a single exercise protocol, and the dose–response relationships between exercise intensity, duration, frequency, and therapeutic efficacy have not yet been determined. Future studies should systematically investigate different exercise prescriptions to define the optimal exercise parameters for enhancing the therapeutic efficacy of U CAR-T cells. Mechanistically, our findings suggest that the CXCL9/CXCR3 signaling axis may be involved in the enhanced antitumor effects of U CAR-T cells induced by aerobic exercise; however, the upstream regulatory mechanisms and interactions with other immune cell populations remain to be elucidated. Future studies integrating single-cell sequencing, spatial transcriptomics, and multi-omics approaches may provide a comprehensive understanding of the processes underlying exercise-induced immune-cell recruitment, inflammatory cytokine modulation, vascular functional improvement, and TME remodeling. In addition, the long-term in vivo persistence of U CAR-T cells, the establishment of immunological memory, and their potential effects on tumor recurrence and metastasis should be further evaluated. These studies may provide a stronger theoretical basis and experimental support for the clinical translation of aerobic exercise combined with universal CAR-T cell therapy.

Conclusion

In conclusion, this study investigated the development of a novel immunotherapeutic strategy for CRC by combining U CAR-T cell therapy with aerobic exercise through a series of in vitro and in vivo experiments. CRISPR/Cas9-mediated knockout of NLRC5 and CIITA in iPSCs generated low-immunogenicity universal iPSCs, from which $CD4^+$ and $CD8^+$T lymphocytes could be differentiated with reduced susceptibility to allogeneic immune recognition, thereby potentially reducing the risk of GVHD and providing a foundation for the scalable generation of U CAR-T cells. A CEA-targeted lentiviral vector was subsequently introduced into these cells to generate U CAR-T cells with stable in vitro expansion and potent, specific cytotoxicity against CEA-positive CRC cells. Furthermore, aerobic exercise increased CXCL9 expression within the TME and was associated with enhanced infiltration of U CAR-T cells into tumor tissues. In a CRC mouse model, the combination of U CAR-T cell therapy and aerobic exercise produced enhanced antitumor effects compared with either treatment alone, while exhibiting favorable tolerability. Collectively, these findings provide experimental evidence for aerobic exercise as a potential adjunctive strategy to enhance U CAR-T cell therapy and suggest a potential therapeutic approach for CRC.

Declarations

Ethics approval and consent to participate

The use of human induced pluripotent stem cells (hiPSCs) in this study was reviewed and approved by Shandong Sport University ethics committee under the project titled ‘Immune Checkpoint Blockade and the Development and Clinical Evaluation of a Universal CEA-Targeted CAR-T Cell Product for Colorectal

Cancer' (Approval No. 2021041; date of approval: 01-12-2021). The hiPSCs were derived from samples donated by healthy donors. Written informed consent for participation in the study and for the use of their samples was obtained from all donors prior to sample collection. All procedures involving human cells were performed in accordance with the principles of the Declaration of Helsinki.

Consent for publication

Not applicable.

Competing interests

The authors declare that they have no competing interests.

Funding

This work was supported by grants from the central government guides local science and technology development funds (YDZX2022091).

Author Contribution

J.Z. and X.Z. designed the study, performed experiments and wrote the main manuscript text. G.Y. assisted with animal experiments and data analysis. Q.W. and S.W. interpreted the data and revised the manuscript. S.W. supervised the whole project. J.Z. prepared Figures 1-7. All authors reviewed and approved the final manuscript.

Acknowledgments

The authors declare that they have not use AI-generated work in this manuscript.

Availability of data and materials

The data supporting the findings of this study are available within the article and its supplementary information files. Any data not included in the article are available from the corresponding author upon reasonable request.

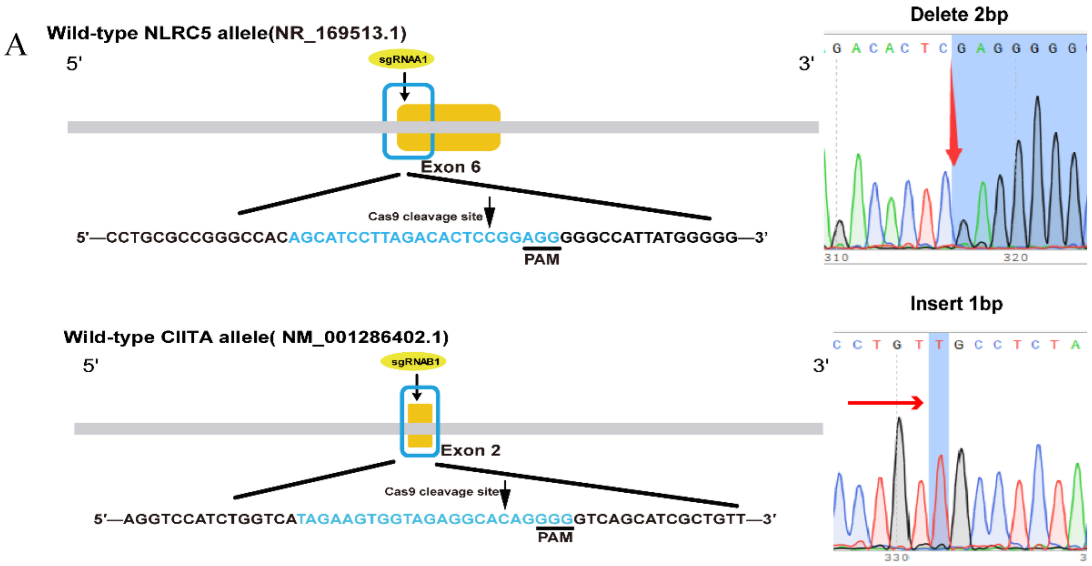
References

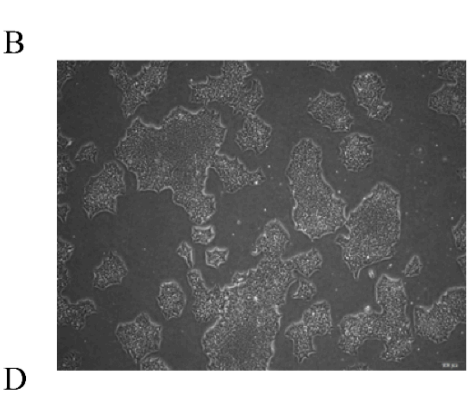
1. Lee DJ, Parikh A, Sirohi B, Cao Y, Chan AT. Emerging trends in the global burden of colorectal cancer. Nat Rev Clin Oncol. 2026;23(8):569–81.
2. Hu R, et al. Advances in intestinal flora for the development, diagnosis and treatment of CRC. Front Microbiol. 2025;16:1495274.
3. Sung H, et al. Global Cancer Statistics 2020: GLOBOCAN Estimates of Incidence and Mortality Worldwide for 36 Cancers in 185 Countries. CA Cancer J Clin. 2021;71(3):209–49.
4. Diao X, et al. Cancer situation in China: an analysis based on the global epidemiological data released in 2024. Cancer Commun (London England). 2025;45(2):178–97.
5. Bray F, et al. Global cancer statistics 2022: GLOBOCAN estimates of incidence and mortality worldwide for 36 cancers in 185 countries. Cancer J Clin. 2024;74(3):229–63.
6. Zhou J, et al. Evolving landscape of colorectal cancer: Global and regional burden, risk factor dynamics, and future scenarios (the Global Burden of Disease 1990–2050). Ageing Res Rev. 2025;104:102666.
7. Yue Y, et al. A novel Senescence-Based prognostic model unveils tumor interactions and drug resistance in colorectal cancer. Int Immunopharmacol. 2024;134:112197.
8. Chen J, et al. Target delivery of a PD-1-TREM2 scFv by CAR-T cells enhances anti-tumor efficacy in colorectal cancer. Mol Cancer. 2023;22(1):131.
9. Bando H, Ohtsu A, Yoshino T. Therapeutic landscape and future direction of metastatic colorectal cancer. Nat Rev Gastroenterol Hepatol. 2023;20(5):306–22.
10. Kung HC, et al. Patterns of recurrence after curative intent hepatic resection for colorectal liver metastasis. J Gastrointest surgery: official J Soc Surg Aliment Tract. 2024;28(12):2031–8.
11. Kajiwara Y, Ueno H. Essential updates 2022–2023: Surgical and adjuvant therapies for locally advanced colorectal cancer. Annals gastroenterological Surg. 2024;8(6):977–86.
12. Gillespie BM, et al. Worldwide incidence of surgical site infections in general surgical patients: A systematic review and meta-analysis of 488,594 patients. Int J Surg (London England). 2021;95:106136.
13. Martino M et al. (2021) A Review of Clinical Outcomes of CAR T-Cell Therapies for B-Acute Lymphoblastic Leukemia. Int J Mol Sci 22(4).
14. Zhang Y, et al. Barriers and Strategies to Enhance CAR-T Cell Infiltration in Solid Tumours: A Systematic Review. Immunology. 2026;178(1):62–78.
15. Sun Q, Long L. Diagnostic performances of methylated septin9 gene, CEA, CA19-9 and platelet-to-lymphocyte ratio in colorectal cancer. BMC Cancer. 2024;24(1):906.
16. Yang Q, et al. Construction of a postoperative liver metastasis prediction model for colorectal cancer based on spectral CT imaging, CEA, and CA19-9. Translational cancer Res. 2025;14(3):2113–24.
17. Li XN et al. (2025) XCL1-secreting CEA CAR-T cells enhance endogenous CD8(+) T cell responses to tumor neoantigens to confer a long-term antitumor immunity. *Journal for immunotherapy of cancer*

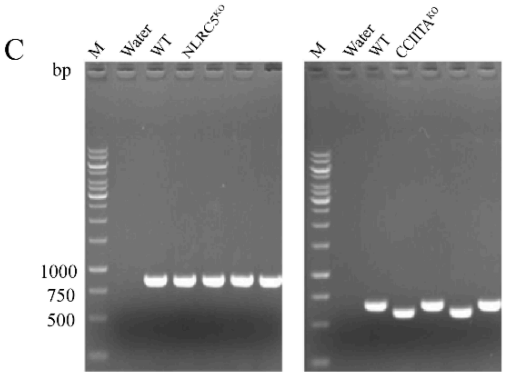
13(1).
18. Jetley U, et al. A differentiated and durable allogeneic strategy applicable to cell therapies. Cytotherapy. 2026;28(3):101991.
19. Su J, et al. Genome-edited allogeneic CAR-T cells: the next generation of cancer immunotherapies. J Hematol Oncol. 2025;18(1):90.
20. Courneya KS, et al. Structured Exercise after Adjuvant Chemotherapy for Colon Cancer. N Engl J Med. 2025;393(1):13–25.
21. Liu L et al. (2026) Exercise and CD8(+) T cells: mechanisms of immune modulation in antitumor responses. J Mol Med 104(1).
22. Lahimchi MR, Maroufi F, Maali A. Induced Pluripotent Stem Cell-Derived Chimeric Antigen Receptor T Cells: The Intersection of Stem Cells and Immunotherapy. Cell reprogramming. 2023;25(5):195–211.
23. Jones RD, et al. Tunable differentiation of human CD4(+) and CD8(+) T cells from pluripotent stem cells. Cell Stem Cell. 2026;33(1):73–e9014.
24. Chen YJ, Abila B, Mostafa Kamel Y. (2023) CAR-T: What Is Next? *Cancers* 15(3).
25. Restle D et al. (2025) Intraperitoneal CAR T-cell therapy for peritoneal carcinomatosis from gastroesophageal cancer: preclinical investigations to a phase I clinical trial (NCT06623396). *Journal for immunotherapy of cancer* 13(9).
26. Kurz E, et al. Exercise-induced engagement of the IL-15/IL-15Rα axis promotes anti-tumor immunity in pancreatic cancer. Cancer Cell. 2022;40(7):720–e737725.
27. Wang B, et al. Generation of hypoimmunogenic T cells from genetically engineered allogeneic human induced pluripotent stem cells. Nat biomedical Eng. 2021;5(5):429–40.
28. Brunschwiler F, Nakka S, Guerra J, Guarda G. A Ménage à trois: NLRC5, immunity, and metabolism. Front Immunol. 2024;15:1426620.
29. Zhu B, Ouda R, An N, Tanaka T, Kobayashi KS. The balance between nuclear import and export of NLRC5 regulates MHC class I transactivation. J Biol Chem. 2024;300(5):107205.
30. Chen L, et al. IL-1β-mediated suppression of CIITA attenuates IFN-γ-induced MHC-II expression on Fibroblasts. Cell communication signaling: CCS. 2025;24(1):25.
31. Krause LCM, et al. The IFNγ-CIITA-MHC II axis modulates melanoma cell susceptibility to NK-cell-mediated cytotoxicity. Mol Oncol. 2025;19(11):3096–119.
32. Du B, et al. CAR-T therapy in solid tumors. Cancer Cell. 2025;43(4):665–79.
33. Escobar G, Berger TR, Maus MV. CAR-T cells in solid tumors: Challenges and breakthroughs. Cell Rep Med. 2025;6(11):102353.
34. Lamplugh ZL, Wellhausen N, June CH, Fan Y. Microenvironmental regulation of solid tumour resistance to CAR T cell therapy. Nat Rev Immunol. 2026;26(3):230–48.
35. Murad JP, et al. Solid tumour CAR-T cells engineered with fusion proteins targeting PD-L1 for localized IL-12 delivery. Nat biomedical Eng. 2026;10(4):613–29.

36. Vitanza NA, et al. Intracerebroventricular B7-H3-targeting CAR T cells for diffuse intrinsic pontine glioma: a phase 1 trial. Nat Med. 2025;31(3):861–8.
37. Chen N, et al. Chimeric Antigen Receptor T Cells Targeting CD19 and GCC in Metastatic Colorectal Cancer: A Nonrandomized Clinical Trial. JAMA Oncol. 2024;10(11):1532–6.

Figures







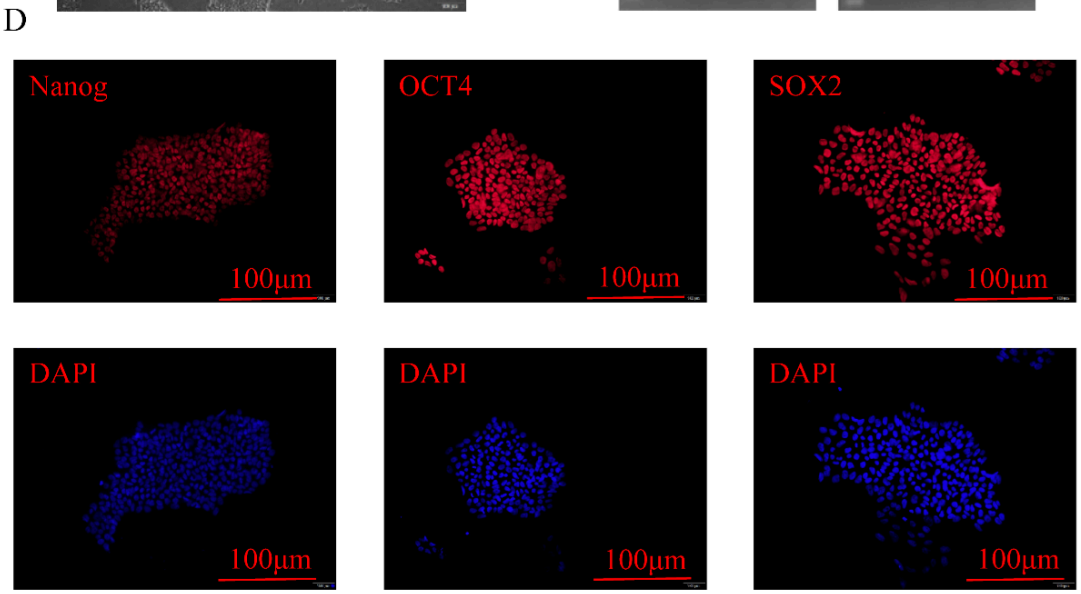


Figure 1

Generation and characterization of NLRC5-CIITA double-knockout (dKO) iPSCs.

(A) Sequence chromatograms showing the genetic variants of NLRC5KO and CIITAKO (dKO) iPSC cell lines. (B) Morphological characteristics of NLRC5-CIITA dKO iPSCs after gene knockout. (C) Agarose gel electrophoresis analysis of BbsI-digested PCR amplification products (1000bp), showing the specific bands corresponding to $NLRC5^{KO}$ (850bp) and $CIITA^{KO}$ (647bp). (D) Immunofluorescence analysis of pluripotency marker expression in the NLRC5-CIITA dKO iPSC cell line.

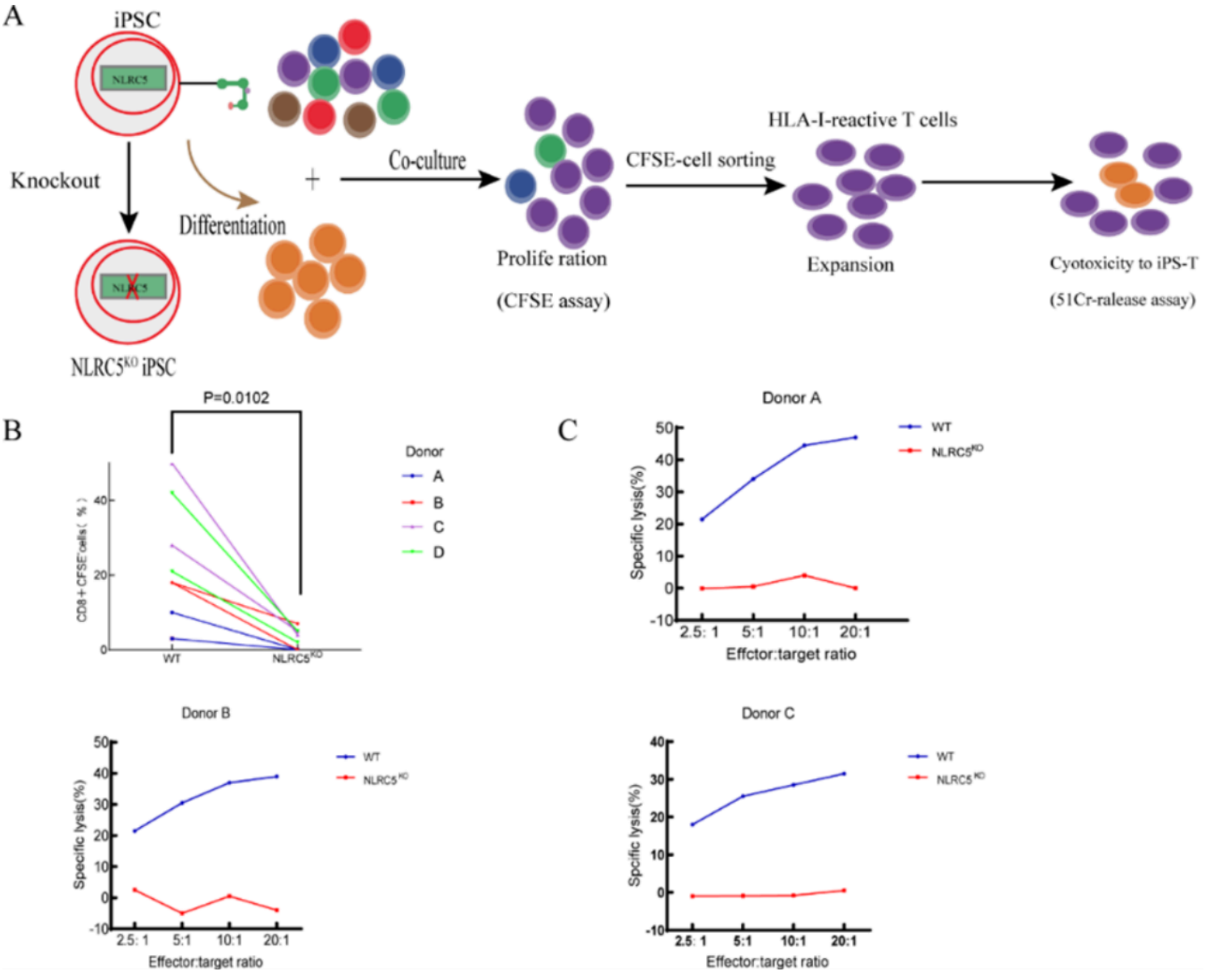


Figure 2

Generation and validation of $NLRC5^{KO}$ iPSC-T cells with reduced immunogenicity and resistance to allogeneic $CD8^{+}$T-cell recognition.

(A) Schematic illustration of the generation strategy for low-immunogenicity NLRC5^{KO} iPSC-T cells.(B) Quantitative analysis of CFSE dilution in allogeneic CD8^{+} T cells co-cultured with parental wild-type (WT) or NLRC5^{KO} iPSC-T cells for 7-8 days (n=4).(C) Cytotoxicity of WT iPSC-T cells and NLRC5^{KO} iPSC-T cells evaluated by the ^{51}Cr release assay after incubation with allogeneic CD8^{+}T cells at effector-to-target (E) ratios of 2.5:1, 5:1, 10:1, and 20:1. Data are presented as mean ± variance. *P<0.05,**P<0.01.

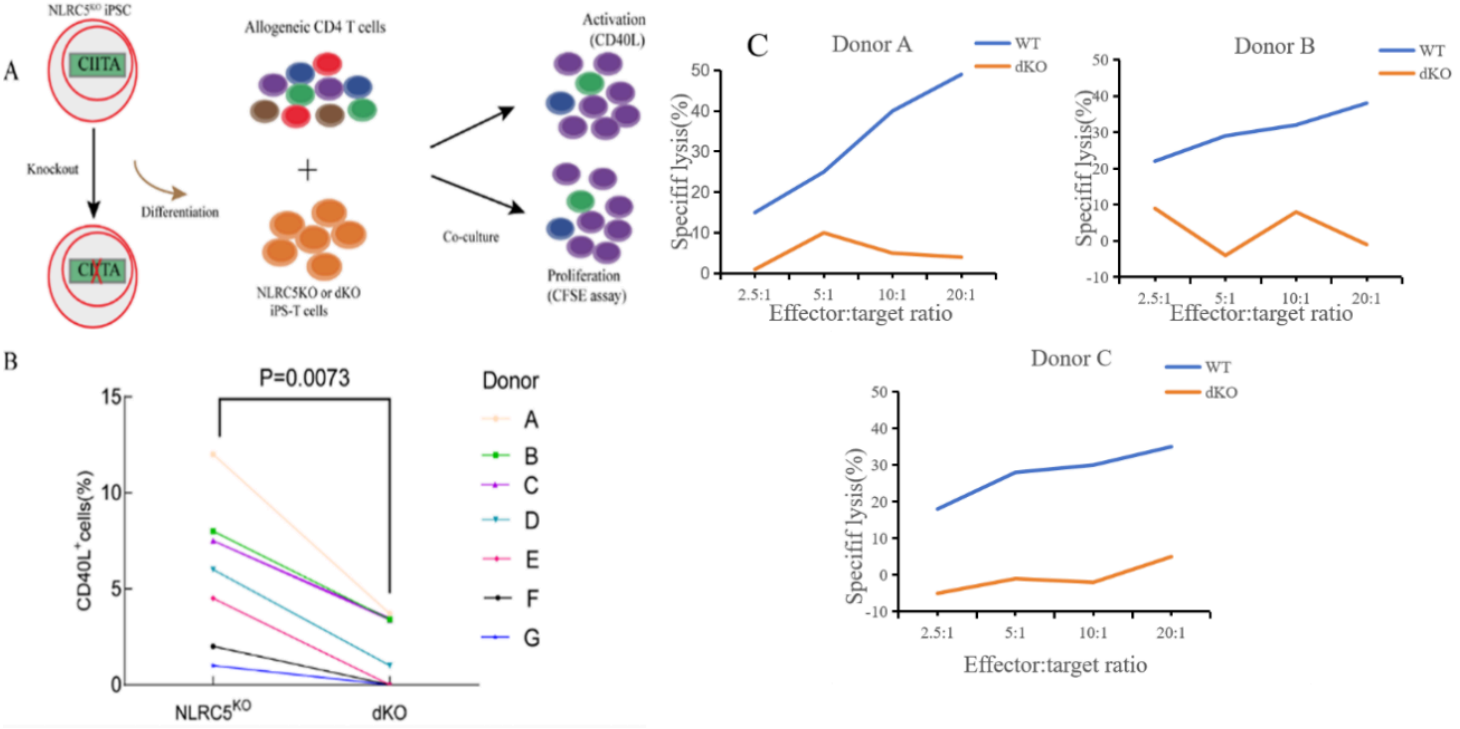


Figure 3

Generation and validation of CIITA knockout iPSC-T cells with reduced immunogenicity against allogeneic CD4^{+}T-cell recognition.

(A) Schematic illustration of the generation strategy for low-immunogenicity CIITA^{KO} iPSC-T cells.(B) Quantitative analysis of CFSE dilution and CD40L expression in allogeneic CD4^{+}T cells co-cultured with HLA-II-expressing CIITA^{KO} iPSC-T cells or dKO iPSC-T cells for 7-8 days (n=7).(C) Cytotoxicity of WT iPSC-T cells and NLRC5^{KO} iPSC-T cells evaluated by the ^{51}Cr release assay after incubation with allogeneic CD4^{+}T cells at effector-to-target (E) ratios of 2.5:1, 5:1, 10:1, and 20:1. Data are presented as mean ± variance. *P<0.05,**P<0.01.

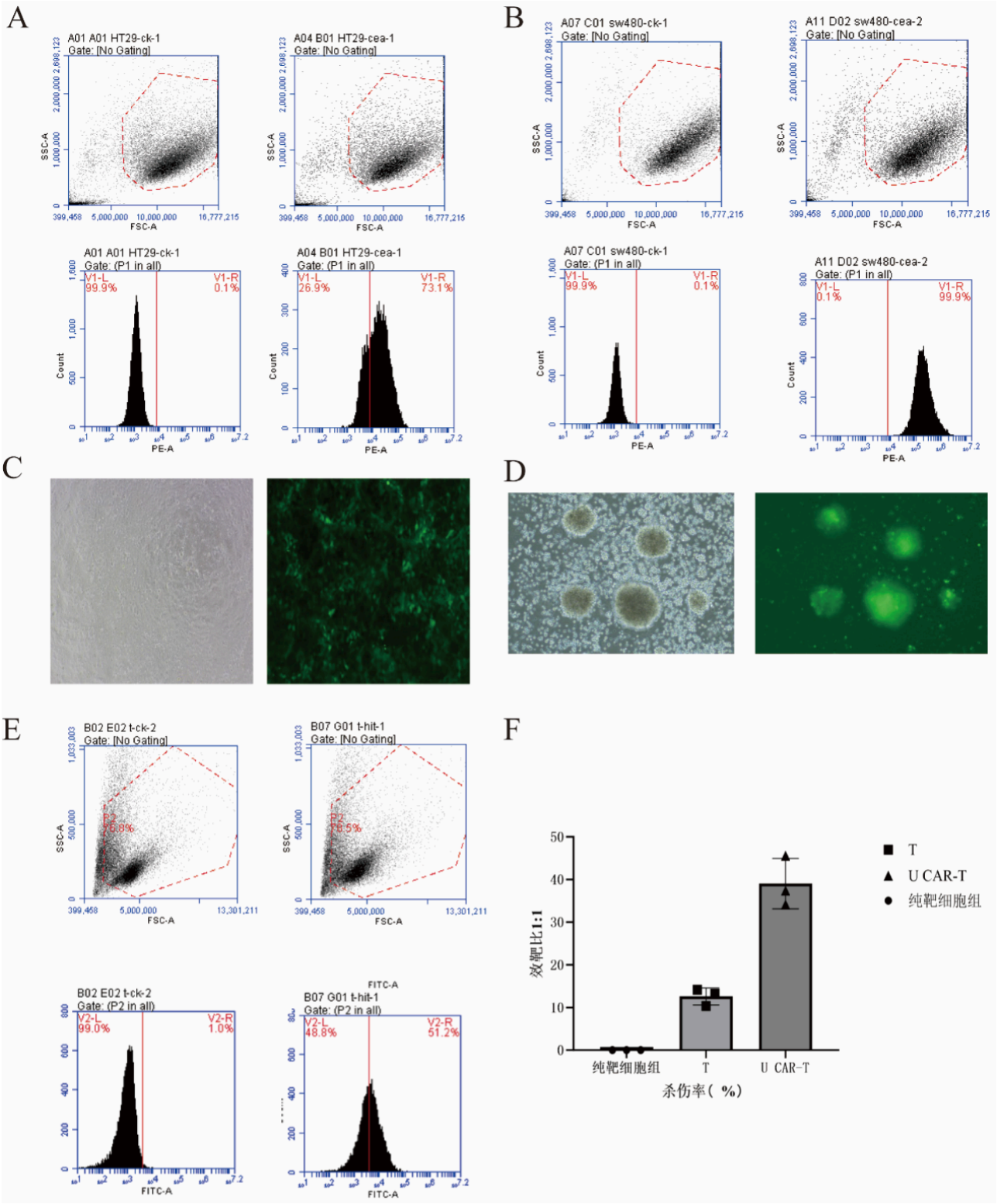


Figure 4

Generation and characterization of universal CEA-CAR-T (U CAR-T) cells.

(A, B) CEA expression in HT-29 and SW480 cells was detected by flow cytometry.(C) Fluorescence microscopy analysis of GFP expression in 293T cells (scale bar=100μm).(D) Immunofluorescence analysis of CEA-CAR expression in U CAR-T cells.(E) Quantitative analysis of U CAR-T cell expression by

flow cytometry.(F) SW480 cells were co-cultured with control T cells or U CAR-T cells at an effector-to-target ratio of 1:1 for 24 h, and the in vitro cytotoxicity of U CAR-T cells was evaluated using the CellTiter-Lumi™ assay.

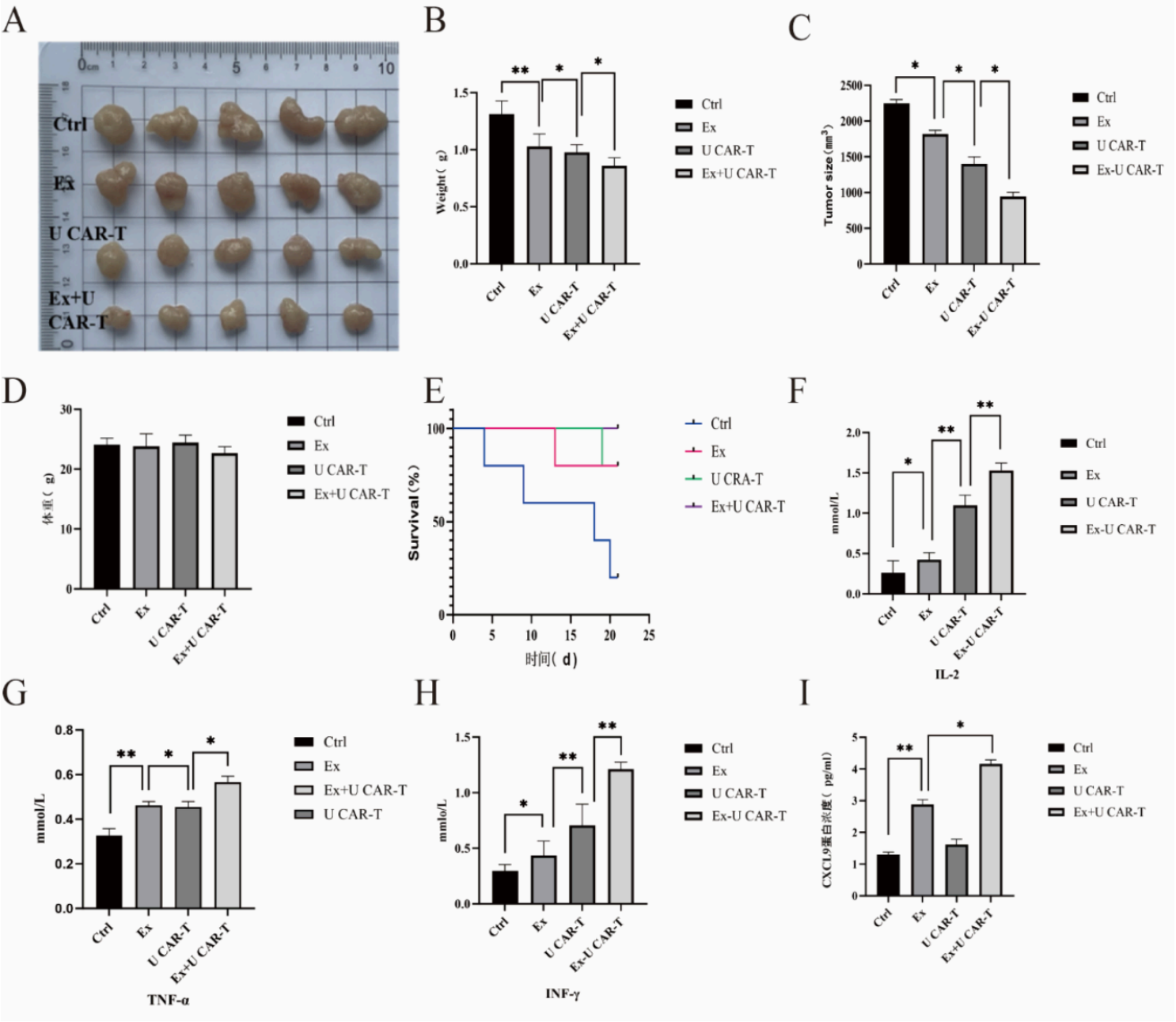


Figure 5

U CAR-T cell therapy delays tumor growth and modulates intratumoral cytokine and CXCL9 protein expression.

(A-C) Tumor volume and body weight in mice (n=5). Six-week-old NYG mice in the U CAR-T and Ex+U CAR-T groups received intraperitoneal injections of 1×10^7 CEA-targeting CAR-T cells per mouse on days 2, 9, and 16 after tumor establishment (n=5), whereas mice in the Ctrl and Ex groups received an equal volume of PBS by intraperitoneal injection once weekly for three consecutive weeks. Mice in the Ex and

Ex+U CAR-T groups underwent aerobic treadmill training for 3 weeks (9 m/min, 30 min/day, 5 days/week).(D) Body weight was measured every 2 days in each group.(E) Effects of different treatment regimens on the survival of CRC-bearing mice.(F-H) Concentrations of intratumoral IL-2, TNF-α, and IFN-γ in each treatment group.(I) CXCL9 protein levels in tumor tissues from each treatment group. Statistical analyses were performed using the unpaired t-test and one-way analysis of variance (ANOVA). Data are presented as mean±variance.*P<0.05,**P<0.01,***P<0.001.

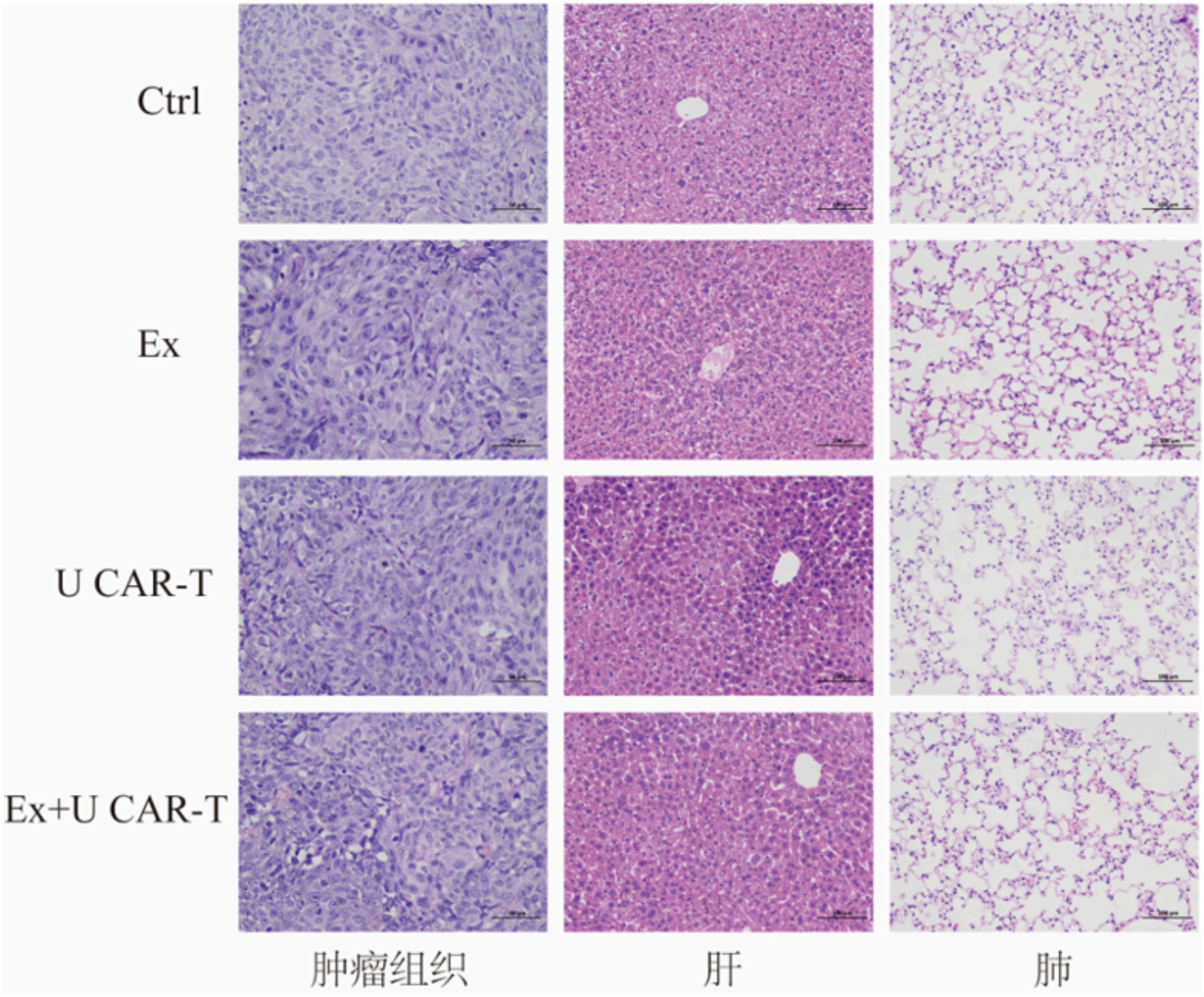


Figure 6

HE staining of tumor, liver, and lung tissues in CRC-bearing mice from each treatment group.

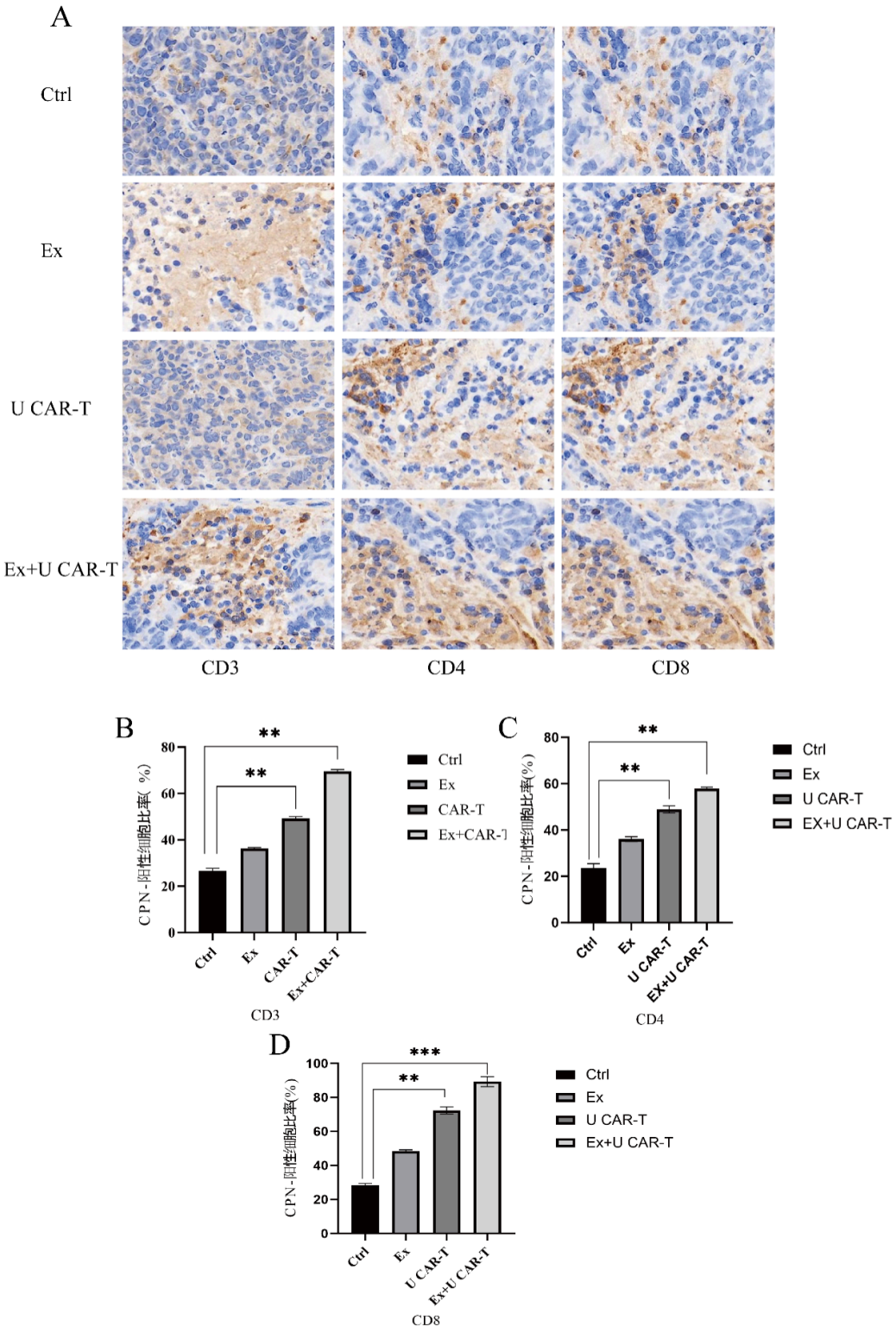


Figure 7

U CAR-T cell therapy regulates the positive staining area and proportion of tumor-infiltrating CD3⁺, CD4⁺, and CD8⁺T cells.

(A) The positive staining areas of tumor-infiltrating $CD3^+$, $CD4^+$, and $CD8^+$T cells were assessed by immunohistochemistry on day 23. The corresponding positive staining areas in the combined-treatment

group were 10.03%, 24.21%, and 38.51%, respectively.(B-D) Proportions of $CD3^+$, $CD4^+$, and $CD8^+$T cells in the different treatment groups. The corresponding positive cell proportions in the combined-treatment group were 71.25%, 58.21%, and 91.55%, respectively. Statistical analyses were performed using the unpaired t-test and one-way analysis of variance (ANOVA). Data are presented as mean ± variance. *P<0.05,**P<0.01,***P<0.001.